

Frequency-Domain Transient Electromigration Analysis Using Circuit Theory

Mohammad Abdullah Al Shohel
University of Minnesota
 Minneapolis, MN, USA
 shohe001@umn.edu

Vidya A. Chhabria
Arizona State University
 Tempe, AZ, USA
 vidyachhabria@asu.edu

Nestor Evmorfopoulos
University of Thessaly
 Volos, Greece
 nestevmo@uth.gr

Sachin S. Sapatnekar
University of Minnesota
 Minneapolis, MN, USA
 sachin@umn.edu

Abstract—The analysis of transient stress buildup in on-chip interconnects due to electromigration (EM) requires the solution of partial differential equations (PDEs) with appropriate boundary conditions, but prior approaches have been computationally expensive. This paper uses a stress-electrical equivalence to map the solution of the system of PDEs for a general multisegment interconnect to an RC network. For tree structures, this system is solved in linear time using model order reduction (MOR) techniques in the frequency domain. We present two MOR approaches: one that is not guaranteed to provide a stable approximant due to the presence of the mass-conservation equation, but empirically does so for a large fraction of testcases; and another that is guaranteed-stable. To achieve a guaranteed-stable solution, the approach approximates the RC circuit in a Krylov space and captures the impact of mass conservation in the form of a mass conservation excitation. However, the latter is observed to be slightly less accurate than the first approach when it does provide a solution. The method demonstrates excellent accuracy against a commercial numerical solver, and is scalable, solving transient EM analysis problems on large power grid interconnect benchmarks.

I. INTRODUCTION

Electromigration (EM) is a reliability failure mechanism that may occur when high currents flow through wires for long periods, e.g., in supply wires in a digital or analog circuit. In older technologies, EM was considered a problem only in upper metal layers that carry the largest current, but in FinFET technologies, as transistors drive increasing amounts of current through narrow wires, EM hotspots have emerged as a significant issue in lower metal layers [1], [2].

Conventional EM analysis, using the Blech criterion [3] to filter out immortal wires, followed by Black’s equation [4] to check EM lifetime, is well known to be flawed for multisegment interconnects. Physics-based EM analysis [5] presents a canonical formulation of one-dimensional EM equations, and has formed the basis of much recent work. Steady-state immortality checks can be performed in linear time [6]–[8], but for the general transient analysis problem, for predicting EM stress over time in multisegment interconnect structures, existing methods [9]–[13], are computationally expensive. Linear time-invariant (LTI) methods have been explored in the time domain [14] as well as in the frequency domain [15], but do not leverage of the efficiencies available in analyzing tree-structured interconnects, and have large runtimes. Recent work [16] achieves low computation times by drawing a

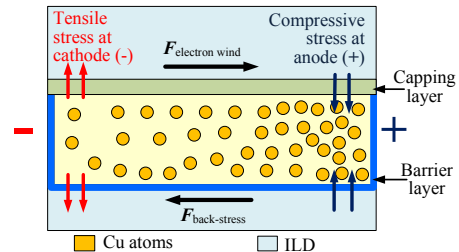


Fig. 1: Illustration of electromigration in a Cu wire [12].

parallel with a stress wave that emanates from each end-point or via in a multisegment interconnect structure, but is only applicable to RC lines without branches.

We propose to perform transient EM analysis in general interconnects in the prenucleation phase through a stress-electrical equivalence that maps Korhonen’s equation for stress [5], and its boundary conditions, to an RC network with current source excitations. The proposed RC mapping is superficially similar to [17], but with a more straightforward translation of the discretized stress equations to lumped RC networks, as well as mapping of the necessary boundary conditions (especially mass conservation) to appropriate excitations. We then solve the resulting RC network by using model order reduction (MOR) techniques in the frequency domain. Unlike prior computationally expensive time-domain solutions, or matrix-based frequency-domain solutions [15], our frequency-domain methods use linear-time graph traversals for trees. Frequency domain solution for the EM problem is nontrivial due to the mass conservation condition, whose application in MOR can lead to unstable reduced-order models. We circumvent this with a two-step solution: we first apply a fast approach that does not guarantee stability, but in practice, often provides stable solutions. If this method fails, we use a second approach that achieves stability but may be less accurate. To our knowledge, this is the first linear-time solution for transient EM stress analysis in interconnect trees.

II. BACKGROUND

Fig. 1 shows the cross-section of a Cu dual-damascene (DD) wire and illustrates the electromigration mechanism in terms of two driving forces i.e. the electron wind force and the back-stress force [5]. When current flows in the wire, the momentum of the electrons drive metal atoms from the cathode towards

the anode, in the direction of electron flow. The movement of migrating atoms is limited to a single metal layer since the barrier layer acts as a blocking boundary for mass transport [18], [19] and prevents atoms from migrating across layers. Due to this electron wind force, the cathode is depleted of metal atoms and a tensile stress is built up near the cathode, which may lead to void formation. Simultaneously, migrating atoms accumulate at the anode terminal and a compressive stress is created near the anode. As metal atoms migrate towards the anode, the resulting concentration gradient (sometimes referred to in the literature as the chemical potential gradient) creates a stress-induced reverse flow of atoms to the cathode. This force, which acts against the electron wind force, is proportional to the stress gradient and known as back-stress.

The temporal evolution of EM-induced stress, $\sigma(x, t)$, at any point in a segment is modeled by the 1-D partial differential equation [5] that relates the stress σ to x , the distance from the cathode:

$$\frac{\partial \sigma}{\partial t} = \frac{\partial}{\partial x} \left[\kappa \left(\frac{\partial \sigma}{\partial x} + \beta j \right) \right] \quad (1)$$

$$\text{where } \beta = \frac{Z^* e \rho}{\Omega}, \quad \kappa = D_a \mathcal{B} \Omega / (kT) \quad (2)$$

Here, j is the wire current density, $Z^* e$ is the effective electron charge, ρ is the resistivity, Ω is the atomic volume for the metal, \mathcal{B} is the bulk modulus of the material, k is Boltzmann's constant, T is the temperature, and $D_a = D_0 e^{-E_a/kT}$ is the diffusion coefficient, with E_a being the activation energy. The thermally-induced stress, σ_T , caused by differentials in the coefficient of thermal expansion in the interconnect stack, is superposed over this stress. Its impact is realized by offsetting the critical stress, σ_{crit} , to $(\sigma_{crit} - \sigma_T)$.

A general interconnect structure consists of a set of *segments* of wires between vias and junctions, each associated with a current density. In general, for a multisegment interconnect structure, currents may be injected (or drawn) at intermediate nodes through vias. For an intermediate node n_i of the structure with degree d_i , we denote the set of incident segments as $S_i = \{s_1, s_2, \dots, s_{d_i}\}$.

Stress evolution in each segment is described by the partial differential equation (1). These equations are supplemented by spatial boundary conditions and a temporal boundary condition that initializes the segment stresses to zero at $t = 0$. The spatial boundary conditions, which must be obeyed over all time points, are [14]:

(1) *Continuity*: For each segment s_k incident on node n_i , if $\sigma_{s_k}|_{n_i}$ is its stress at n_i , then continuity of stress implies that:

$$\sigma_{s_1}|_{n_i} = \sigma_{s_2}|_{n_i} = \dots = \sigma_{s_{d_i}}|_{n_i} \quad (3)$$

(2) *Flux*: The net atomic flux entering each node n_i is zero:

$$\sum_{s_k \in S_i} w_{s_k} \tau_{s_k} \left(\frac{\partial \sigma_{s_k}}{\partial x} \Big|_{n_i} + \beta j_{s_k} \right) = 0 \quad (4)$$

where S_i is the set of segments incident on n_i , j_{s_k} is the current density through segment s_k (leaving n_i), and w_{s_k} and τ_{s_k} are, respectively, the segment width and thickness. At an end point of degree 1, this reduces to $\frac{\partial \sigma}{\partial x} \Big|_{n_i} + \beta j_{s_k} = 0$.

(3) *Mass conservation*: This conserves the flux over the interconnect:

$$\sum_{\text{all segments } s_k} \iiint \sigma_{s_k}(x) dx dw d\tau = 0 \quad (5)$$

where $\sigma_{s_k}(x)$ is the stress at location x in segment s_k . The triple integral is taken over the volume of each segment s_k .

III. PROBLEM FORMULATION

A. The Stress-Electrical Analogy

Each segment in an interconnect structure is assumed to carry a constant current density j [7], [14]. Therefore, $\partial(\beta j)/\partial x = 0$, and Korhonen's equation (1) for each segment becomes:

$$\frac{\partial \sigma}{\partial t} = \kappa \frac{\partial^2 \sigma}{\partial x^2} \quad (6)$$

We present an equivalent circuit model for this structure. The model is functionally similar to [17], which also shows a transmission line formulation, but we believe our exposition more intuitively uses κ as a "stress conductivity," and also provides a more intuitive explanation of boundary conditions (BCs).

The form of (6) is similar to the heat equation, which is well-known to admit a thermal-electrical analogy [20]. The parameter κ replaces thermal conductivity and can be called the *stress conductivity* in this context. Using a similar principle, we derive a *stress-electrical analogy* that maps the solution of the electromigration problem to one of performing transient analysis on an RC network. We use a uniform discretization similar to the finite difference method, where for each element i of size Δx , the function $\sigma(x, t)$ is discretized assuming a uniform stress $\sigma_i(t)$ for all points within the element.

Fig. 2 shows three consecutive discretized elements, $i-1$, i , and $i+1$, in a two-segment line. Using a finite difference to approximate the spatial derivative, (6) becomes:

$$\frac{d\sigma_i}{dt} = \kappa \frac{\left(\frac{\sigma_{i+1} - \sigma_i}{\Delta x} \right) - \left(\frac{\sigma_i - \sigma_{i-1}}{\Delta x} \right)}{\Delta x} \quad (7)$$

$$(\Delta x \cdot w \cdot \tau) \frac{d\sigma_i}{dt} = \kappa \left(\frac{\sigma_{i+1} - \sigma_i}{\Delta x / (w \cdot \tau)} \right) - \kappa \left(\frac{\sigma_i - \sigma_{i-1}}{\Delta x / (w \cdot \tau)} \right) \quad (8)$$

where w and τ are the width and thickness of the wire segment that the element belongs to. The partial derivative with respect to time in (6) becomes the ordinary derivative in (8), since after discretization, σ_i in each element i depends only on time.

Now consider the electrical circuit shown in the lower half of Fig. 2. The circuit equation at each node i is given by

$$CdV_i/dt = ((V_{i+1} - V_i)/R) - ((V_i - V_{i-1})/R) \quad (9)$$

Comparing (8) and (9), for each element of length Δx , the discretized stress equation has a direct mapping to the electrical circuit. We summarize the stress-electrical relation using the equivalences:

$$\sigma \leftrightarrow V ; (\Delta x \cdot w \cdot \tau) \leftrightarrow C ; \frac{1}{\kappa} \frac{\Delta x}{(w \cdot \tau)} \leftrightarrow R \quad (10)$$

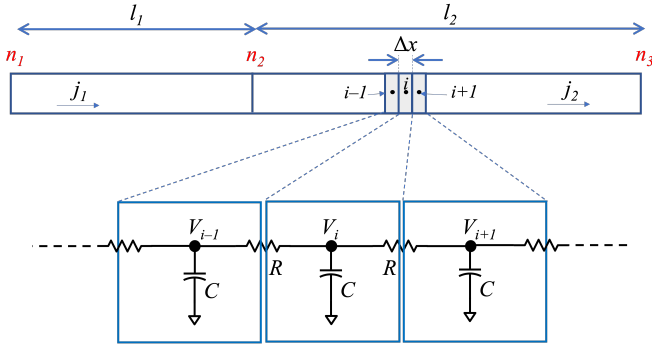


Fig. 2: A few discretized elements in a two-segment line, and the RC equivalent structure around element i .

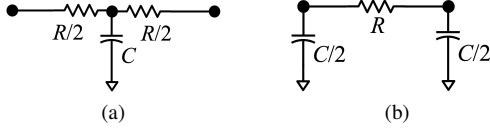


Fig. 3: (a) A T-model for each discretized element of the line, based on Fig. 2. (b) An equivalent π -model.

where V , R , and C are the electrical voltage, resistance, and capacitance, respectively. Note that the stress resistance has the familiar form of the electrical resistance of a conducting material of length Δx , cross-section $(w \cdot \tau)$ and resistivity $\frac{1}{\kappa}$, while the stress capacitance is equal to the volume $(\Delta x \cdot w \cdot \tau)$ of the element.

Thus, stress analysis of a multisegment interconnect structure is translated into analysis of an RC circuit analysis with current sources arising from BCs (as shown in the next subsection). The stress-electrical analogy opens the doors to mapping transient EM analysis to transient RC circuit analysis, which has been well studied in the context of timing analysis in IC design [21], [22].

The discretization in Fig. 2 is similar to the familiar T-model used in interconnect analysis: each discretized element maps to the T-structure shown in Fig. 3(a). Equivalently, a π -model may be used, as shown in Fig. 3(b) [23].¹ We choose to use the latter model in this work. In this case, each element is represented using two nodes, one at each edge of the element, with capacitors of value $C/2$ connected to each node and a resistor of value R connecting the nodes. By representing each element by this π -model, an RC equivalent network may be built for stress analysis.

B. Applying Boundary Conditions

The temporal BC sets all initial stresses to 0. The spatial BCs are:

¹The π -model can also be derived directly. We take two nodes $i+1$ and i at the end points of an element, and create a node i' at the center point. We can then write the stress and its derivative at node i' as the average of the values at the two ends. The stress equation is discretized as:

$$\frac{1}{2} \left(\frac{d\sigma_{i+1}}{dt} + \frac{d\sigma_i}{dt} \right) = \kappa \left[\left(\frac{\sigma_{i+1} - \frac{\sigma_{i+1} + \sigma_i}{2}}{\Delta x / (w \cdot \tau)} \right) - \left(\frac{\frac{\sigma_i + \sigma_{i-1}}{2} - \sigma_{i-1}}{\Delta x / (w \cdot \tau)} \right) \right]$$

The remainder of the derivation is similar to that for the T-model.

(1) *Continuity*: Since the end points of adjacent RC segments are connected to the same node, they have the same voltage (\Leftrightarrow stress). The electrical circuit thus naturally satisfies continuity. (2) *Flux*: The flux constraints do not map to those in the traditional statement of the thermal problem, where the Dirichlet-type BC specifies one node “voltage” as the ambient temperature, or reference. For the EM problem, the BCs at the end points of each segment of the structure, given by Equation (4), are Neumann-type where the derivative of the stress, $\partial\sigma/\partial x$, is specified. For the discretized line with elements of size Δx , we can use the stress-electrical equivalence (10) to relate the stress derivative and the current, I , through an element in the equivalent electrical circuit:

$$\kappa \cdot (w \cdot \tau) \frac{\partial\sigma}{\partial x} \approx \kappa \frac{\Delta\sigma}{\Delta x / (w \cdot \tau)} \Leftrightarrow \frac{\Delta V}{R} = I \quad (11)$$

where $\Delta\sigma$ and ΔV are, respectively, the stress differential and the voltage drop across the element of size Δx .

Consider the node n_i in the interconnect structure, and as before, let S_i be the set of segments incident on the node. The BC (4) at n_i can be written as

$$\kappa \sum_{s_k \in S_i} w_{s_k} \tau_{s_k} \frac{\partial\sigma_{s_k}}{\partial x} \Big|_{n_i} + \kappa\beta \sum_{s_k \in S_i} w_{s_k} \tau_{s_k} j_{s_k} = 0 \quad (12)$$

Using (11) and $i_{s_k} = w_{s_k} \tau_{s_k} j_{s_k}$, this maps to:

$$\chi \sum_{s_k \in S_i} I_{s_k} + \kappa \cdot \beta \sum_{s_k \in S_i} i_{s_k} = 0 \quad (13)$$

Note that the first term comes from an equivalence rather than an equality: χ is a scale factor of magnitude 1 that converts the units of the first term to be consistent with those of the second. For ease of readability, we will drop the term χ in the rest of our discussion. The second term is the algebraic sum of the EM stress current leaving the node n_i , over all segments s_k incident on the node.

The boundary condition (4) must hold for all time points, and thus also for $t \rightarrow \infty$ where stress reaches steady state in all segments and $\frac{\partial\sigma}{\partial t} = 0$ at all spatial points. This translates to DC state in the equivalent electrical circuit, where all capacitors at the discretized nodes are opened.

This means that the above equation effectively represents Kirchhoff’s current law (KCL) for node n_i in the equivalent electrical circuit at DC, and thus at any node of the RC structure corresponding to the end point of a segment, a current source of $(\kappa \cdot \beta \sum_{s_k \in S_i} i_{s_k})$ must be connected to ensure that KCL is satisfied at DC. At internal nodes of a segment that are not endpoints, the algebraic sum of i_{s_k} is zero, and no current source is needed.

(3) *Mass conservation*: Under 1-D analysis, where the length of a wire is typically much larger than its width w_s or thickness τ_s , we use a discretization element that spans the entire width and thickness dimensions. We compute the integral in the mass conservation BC (5) as a finite sum over all elements j , which maps to the following electrical equivalent:

$$\sum_j \sigma_j \cdot \Delta x \cdot w_j \cdot \tau_j = 0 \Leftrightarrow \sum_j V_j \cdot \Delta x \cdot w_j \cdot \tau_j = 0 \quad (14)$$

From (10), $\Delta x \cdot w_j \cdot \tau_j = C_j$, the capacitance of element j . Under the π -model, V_j (the element voltage) can be taken

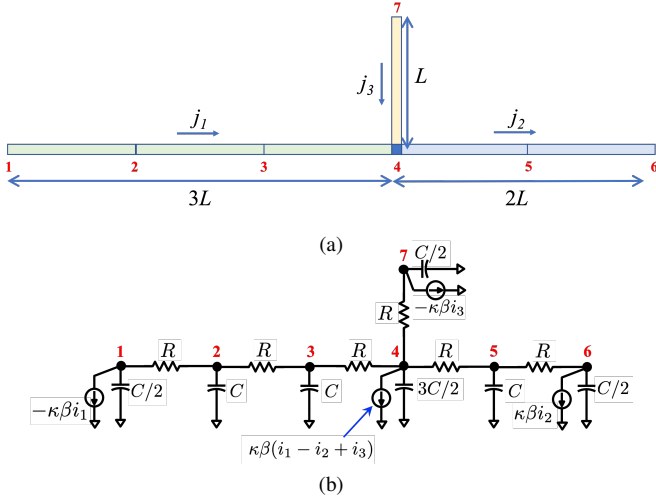


Fig. 4: (a) A three-segment tree discretized into elements. (b) The equivalent RC circuit with excitations.

as the average of the voltages at the two nodes at the end of each element. Therefore, the node voltage at each node k is multiplied by $C_k = \sum C_j/2$ (the capacitance at the node under the π -model); the summation is taken over all elements j incident on the node; in other words, C_k is the total capacitance at node k in the electrical circuit. The equation for mass conservation maps to the electrical domain as

$$\sum_{\text{nodes } k} C_k V_k = 0 \quad (15)$$

C. Example: Electrical Equivalent Model

We illustrate a mapping of the stress problem to an equivalent electrical network, based on the above principles. Our illustrative example is the three-segment tree of Fig. 4(a), with uneven segment lengths, equal segment widths and thicknesses, and with current densities j_1 , j_2 , and j_3 , as shown in the figure.

After discretization into elements of length L , from the stress-electrical equivalence (10), we can build the equivalent RC circuit shown in Fig. 4(b), where each discretized element has identical resistance R and identical capacitance C . The current sources correspond to the flux BCs, as described in the previous subsection. Current sources are added to nodes that correspond to segment end-points. The current source values at the segment end nodes are equal to the algebraic sum of the stressing currents on segments incident on those nodes. The nodal equations for the RC circuit can be written as:

$$C \begin{bmatrix} \frac{1}{2} & 0 & 0 & 0 & 0 & 0 & 0 \\ 0 & 1 & 0 & 0 & 0 & 0 & 0 \\ 0 & 0 & 1 & 0 & 0 & 0 & 0 \\ 0 & 0 & 0 & \frac{3}{2} & 0 & 0 & 0 \\ 0 & 0 & 0 & 0 & 1 & 0 & 0 \\ 0 & 0 & 0 & 0 & 0 & \frac{1}{2} & 0 \\ 0 & 0 & 0 & 0 & 0 & 0 & \frac{1}{2} \end{bmatrix} \begin{bmatrix} V_1 \\ V_2 \\ V_3 \\ V_4 \\ V_5 \\ V_6 \\ V_7 \end{bmatrix} + \frac{1}{R} \begin{bmatrix} 1 & -1 & 0 & 0 & 0 & 0 & 0 \\ -1 & 2 & -1 & 0 & 0 & 0 & 0 \\ 0 & -1 & 2 & -1 & 0 & 0 & 0 \\ 0 & 0 & -1 & 3 & -1 & 0 & -1 \\ 0 & 0 & 0 & -1 & 2 & -1 & 0 \\ 0 & 0 & 0 & 0 & -1 & 1 & 0 \\ 0 & 0 & 0 & -1 & 0 & 0 & 1 \end{bmatrix} \begin{bmatrix} V_1 \\ V_2 \\ V_3 \\ V_4 \\ V_5 \\ V_6 \\ V_7 \end{bmatrix} = \kappa\beta \begin{bmatrix} i_1 \\ 0 \\ 0 \\ -i_1 + i_2 - i_3 \\ 0 \\ -i_2 \\ i_3 \end{bmatrix} \quad (16)$$

The conductance matrix G in (16) is singular (since its rows and columns add up to 0), which is a consequence of the

fact that the RC equivalent circuit has no resistive path to ground (or to a reference voltage). This will make the DC equations needed for the computation of circuit moments (and order reduction) linearly dependent. Here one equation can be removed, say the last, and be replaced by the equation (15) related to mass conservation [15], in order to make the DC system solvable. For this particular example, the additional mass conservation constraint (15) is:

$$\frac{CV_1}{2} + CV_2 + CV_3 + \frac{3CV_4}{2} + CV_5 + \frac{CV_6}{2} + \frac{CV_7}{2} = 0$$

IV. FREQUENCY DOMAIN SOLUTION

We approximate the circuit in the frequency domain using model order reduction (MOR) techniques. MOR methods, including Arnoldi methods, have been extensively explored to approximate the voltage response of an RC interconnect in timing analysis. However, there are significant differences between the EM and timing analysis problems.

(1) For timing analysis, a first-order asymptotic waveform evaluation (AWE) reduction guarantees a stable solution, because the response has a single time constant that is the nonnegative Elmore delay [22]. For the stress problem, the first moment can be negative, and it is easy to construct cases with an unstable first-order approximant.

(2) For the EM problem, all resistors are separated from ground by a cutset of capacitors and current sources (Fig. 4(b)). For the DC state (encountered in moment computation) where all capacitors are open-circuited, there exists a cutset of current sources (whose voltage can be arbitrary) which implies that there is no reference potential in the circuit that uniquely defines all node voltages. This reference level is determined by the mass conservation equation (15), which is not represented in the circuit in Fig. 4(b). In contrast, in timing analysis, since a voltage source is connected directly to the driving point, all node voltages are uniquely defined in the DC state.

Thus, our system is not a traditional timing analysis RC circuit since it also includes the mass conservation constraint. If (as done in [15]) we create a conductance matrix G_{new} and a capacitance matrix C_{new} by replacing one equation (e.g., the last row in (16)) by the conservation of mass equation, then G_{new} is not guaranteed to be positive definite (nor is symmetric), as required for stability [24].

Our two-step approach solves these equations in linear time: *Step 1:* We create the reduced-order model via linear-time tree traversals, similarly to timing analysis [24], but with an extra step to incorporate mass conservation. This solution has no guarantees of stability, but we find that in practice, instability is seen in a very small fraction of testcases, and when the solution is stable, it is accurate.

Step 2: For the few unstable cases (detected by checking the signs of the poles in Step 1), we develop a guaranteed-stable method. It is possible to use this approach for all EM analyses, but empirically, this (still linear-time) approach has

more runtime and lower accuracy than the method in Step 1 (if Step 1 yields a stable approximation).

A. Step 1: MOR without Guaranteed Stability

The work in [15] appended mass conservation constraints to the set of equations. However, their solution involved matrix operations, which do not scale well. In this section, we show how this system can be reduced to a lower order using MOR using a linear-time method based on tree traversals. As mentioned earlier, this is a nontrivial extension of RC timing analysis due to the mass conservation constraint.

We start with the frequency domain representation of the RC circuit equivalent of the stress analysis problem, without the mass conservation equation, which is obtained by the Laplace transform of the nodal equations (e.g. (16)) and can be written as

$$(G + sC)\mathbf{V}(s) = \mathbf{B}e(s) \quad (17)$$

where G and C are, respectively, the node conductance and capacitance matrices; $\mathbf{V}(s)$ is the vector of unknown node voltages; \mathbf{B} is a vector containing the algebraic sums of stressing currents incident at every node (which form the current source magnitudes); and $e(s)$ is the Laplace transform of a unit step excitation function. The part of (17) that does not contain the excitation $e(s)$ (i.e., when assuming a unit impulse $e(s) = 1$) is a circuit transfer function $\mathbf{V}(s) = (G + sC)^{-1}\mathbf{B}$, and can be reduced by MOR to obtain a reduced-order model, on which the time-domain excitation (here a unit step function) can be applied afterwards to simulate stress at specific nodes. To apply MOR we can use standard techniques [25] to find the moments \mathbf{m}_i in the expansion $\mathbf{V}(s) = \sum_i \mathbf{m}_i s^i$, as:

$$G\mathbf{m}_0 = \mathbf{B}; \quad G\mathbf{m}_{i+1} = -C\mathbf{m}_i, i \geq 0 \quad (18)$$

Efficient moment computation for an RC tree. For an RC tree structure, each of the moment vectors \mathbf{m}_i can be computed as the node voltages in a sequence of DC circuits, using tree traversals. To solve for \mathbf{m}_0 in (18), all capacitors are open-circuited and current sources with values equal to the algebraic sums of stressing currents at every node (to form the vector \mathbf{B}) are applied to the resulting DC circuit. For $\mathbf{m}_{i+1}, i \geq 0$, each capacitor C_k to ground at every node k is replaced by a current source of value $(-C_k m_{i,k})$, where $m_{i,k}$ is the k^{th} component of \mathbf{m}_i . These transformations are illustrated in Fig. 5 for the example structure and equivalent circuit of Fig. 4.

Incorporating mass conservation. Combining $V_k(s) = \sum_i m_{i,k} s^i$ for the voltage at node k with mass conservation (15),

$$\sum_{\text{nodes } k} C_k \cdot (m_{0,k} + m_{1,k}s + m_{2,k}s^2 + \dots) = 0 \quad (19)$$

Since this relation holds for all values of s ,

$$\sum_{\text{nodes } k} C_k \cdot m_{i,k} = 0 \quad \forall i \geq 0 \quad (20)$$

Dealing with the absence of reference potential. Since no reference potential is specified in the DC circuits² (18), we

²Each DC circuit for moment computation has a cutset of current sources (\Leftrightarrow capacitors) to ground, and thus the moments are not uniquely solvable.

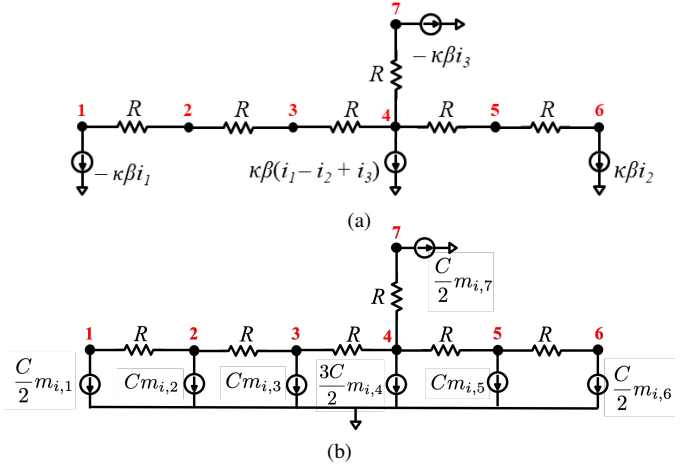


Fig. 5: (a) The equivalent circuit for computing the first moment, \mathbf{m}_0 , for the example in Fig. 4. (b) The equivalent circuit for computing the $(i + 1)^{\text{th}}$ moment, \mathbf{m}_{i+1} .

designate a reference node in the structure and find all voltages as offsets from that reference node. Without loss of generality, if node 1 is the reference, m_i^* , then a pair of tree traversals can compute all voltages \Leftrightarrow moments, $m_{i,k}^0$ relative to the reference. The true value of the moment at node k is obtained by translating it by m_i^* , i.e.,

$$m_{i,k} = m_i^* + m_{i,k}^0 \quad (21)$$

We substitute Equation (21) into Equation (20) to obtain

$$m_i^* = -\frac{\sum_{k=1}^n C_k m_{i,k}^0}{\sum_{k=1}^n C_k} \quad (22)$$

Substituting this into (21) yields the moments of the system. **Constructing the reduced-order model.** We use the PRIMA approach [24] and intersperse the above tree-traversal-based moment calculation with an orthogonalization step that creates an orthogonal basis, which is then used to create a reduced p^{th} order model (by computing p orthogonalized moments). The procedure consists of the following steps (the reader is referred to [24] for details):

- Determine p moments \mathbf{m}_i , as described previously.
- Orthogonalize the moments using a Gram-Schmidt process to obtain an $n \times p$ orthogonal Krylov basis matrix, X .
- Generate a reduced order model

$$(\tilde{G}_{new} + s\tilde{C}_{new})\tilde{\mathbf{V}}(s) = \tilde{\mathbf{B}}e(s),$$

$$\mathbf{Y}(s) = \tilde{L}\tilde{\mathbf{V}}(s)$$

where $\tilde{G}_{new} = X^T G_{new} X$, $\tilde{C}_{new} = X^T C_{new} X$, $\tilde{\mathbf{B}} = X^T \mathbf{B}$, $\tilde{L} = LX$, $\tilde{\mathbf{V}}$ is the $p \times 1$ reduced-order state vector, and L is an $r \times n$ matrix that selects r out of the n nodes in the RC circuit (i.e. discrete points in the interconnect structure) where stress measurements \mathbf{Y} are to be made.

The reduced-order model is small enough that it can be solved directly to obtain the transient response of the equivalent circuit, and compute stress at a desired subset of nodes of the structure. In practice, we find that a low-order model

(of order $p \leq 4$) provides excellent accuracy, and yields stable approximations in most, but not all, testcases (Section V).

Computational complexity: The cost of finding the reduced-order model for a tree structure is linear in the number of tree nodes [21].

B. Step 2: MOR with Guaranteed Stability

The formulation in Step 1 effectively combines mass conservation with the RC circuit equations, which can potentially lead to unstable reduced-order models. We now show how we can avoid this instability by superposing the results of two separate analyses, each guaranteeing passivity of the reduced-order model (and thus also stability) of the numerical solution, by superposing two analysis steps described below: Analysis A ignores mass conservation, while Analysis B captures this constraint using a “mass conservation excitation.” Each analysis solves a problem that maps onto timing analysis, and the solution *inherits guarantees of passivity*.

Analysis A. This step ignores mass conservation (i.e., it uses G rather than G_{new}). As the system of circuit equations is not independent (see the example in (16)), we first designate a reference node (e.g., node 1 in Fig. 4) as ground: removing the corresponding entries from the singular G converts it to a nonsingular matrix G' , and find the moments of the transfer function using a Krylov space method (like PRIMA) on a standard RC circuit, characterized by $A = -G'^{-1}C$. Without mass conservation, the problem maps directly to MOR for timing analysis, and the structure of the computations here is identical to the first part of Step 1. For Analysis A, we will use $M_{i,k}^A$ to denote the i^{th} computed moment at node k .³

Analysis B. Due to mass conservation, using the notation in Step 1, the voltage (\Leftrightarrow stress) at the reference node is not zero (as assumed in Analysis A), but has an i^{th} moment of m_i^* (and hence all moments in Step 1 are shifted by m_i^* in (21)). The true voltage at the reference node is, in fact, represented by the voltage moments as $\sum_i m_i^* s^i$. This observation motivates an alternative interpretation of stress analysis, where the excitations can be split into two: $e(s) = u(s)$, the Laplace transform of the unit step excitation $u(s) = 1/s$ that activates the current sources in each wire, and a “mass conservation excitation” of value $(\sum_i m_i^* s^i)u(s)$ at the reference node, which enforces the mass conservation equation.⁴ A superposition of the two responses provides the solution to the problem. Next, we find the response to the corresponding impulse excitations $e(s) \equiv \delta(s) = 1$ and $\sum_i m_i^* s^i$ and superpose them.

When we apply a unit impulse at the reference node, the response at each node k is the transfer function to that node, denoted as $\sum_i V_{i,k} s^i$. Note that $V_{0,k} = 1 \forall$ nodes k for an RC circuit with no resistive paths to ground [22].

³Note that $M_{i,k}^A \neq m_{i,k}^0$ except for the zeroth moment ($i = 0$), because successive moments in Step 1 incorporate the mass conservation constraint into their moments, while Analysis A is completely free of mass conservation.

⁴It is essential to treat the stress at the reference, $\sum_i m_i^* s^i$, as an excitation; it is not sufficient to simply shift the moments from Analysis A by the time-domain stress at the reference, as in (21). This is because this is not a simple DC shift, but a time-varying voltage excitation that affects the voltages at other nodes. This is consistent with the observation in footnote 3 that $M_{i,k}^A \neq m_{i,k}^0$.

The superposed impulse response of the stress at node k is:

$$\left[\left(\sum_i M_{i,k}^A s^i \right) + \left(\sum_i m_i^* s^i \right) \left(\sum_i V_{i,k} s^i \right) \right]$$

where the first term comes from Analysis A, and the second term is the response to the mass conservation excitation. Since the summation of these terms over all vertices must be zero to obey mass conservation, the coefficient of each power of s must be zero. For the lowest power of s above, using a process similar to (15), the sum of the capacitance-moment products over all nodes is zero. Thus,

$$\sum_k C_k M_{0,k}^A + m_0^* \sum_k C_k V_{0,k} = 0 \Rightarrow m_0^* = -\frac{\sum_k C_k M_{0,k}^A}{\sum_k C_k} \quad (23)$$

where the last equality uses $V_{0,k} = 1 \forall k$. Using a similar approach for the coefficients s^j , it can be shown that

$$m_j^* = -\frac{\sum_k C_k M_{j,k}^A + \sum_{l=0}^{j-1} m_l^* \sum_k C_k V_{j-l,k}}{\sum_k C_k} \quad (24)$$

From (23) and (24), the moments of the mass conservation excitation are in a Krylov space characterized by $A = -G'^{-1}C$; therefore, a passive approximation to the excitation is obtained by PRIMA, and the excitation is stable. In addition, the reduced order model for the circuit is obtained from the same Krylov space as Analysis A, and is hence stable. In short, mass conservation, the potential cause of instability in the approach in Step 1, is moved to an excitation in Analysis B and represented by a low-order rational approximation.

The responses from Analysis A and Analysis B are superposed to obtain the stress at each node. Each analysis is performed using PRIMA [24], where, for tree structures, the moments are computed using tree traversals, followed by orthogonalization steps to build the basis for the Krylov space. Thus, trees are solved in linear time.

V. RESULTS

We present three sets of results to illustrate the accuracy and scalability of our approach. Section V-A first demonstrates our methodology and shows comparisons of our approach with the FEM-based numerical solver, COMSOL, for a six-segment Cu DD interconnect tree. Next, in Section V-B we employ our algorithm on a multibranch interconnect tree of consecutive T -junctions to demonstrate the linear time. Finally, in Section V-C we apply our algorithm to perform EM stress analysis on large-scale power grid benchmarks.

We assume interconnect structures to be built using Cu DD wires: since there is no mass transfer across vias, each layer is analyzed independently. The interconnect specifications [1], [11] used in all our simulations are: $\rho = 2.25\text{e-}8\Omega\text{m}$, $\mathcal{B} = 28\text{GPa}$, $\Omega = 1.18\text{e-}29\text{m}^3$, $D_0 = 1.3\text{e-}9\text{m}^2/\text{s}$, $E_a = 0.8\text{eV}$, $Z^* = 1$, $\sigma_{crit} = 41\text{MPa}$, $T = 378\text{K}$. Since the thermal stress, σ_T , can be computed independently and superposed over the stress computed here, without loss of generality we assume $\sigma_T = 0$ everywhere. Our method is implemented using

Python3.6, and run times are reported on a machine with 128GB RAM and a 2.2GHz Intel® Xeon® Silver 4114 CPU.

A. Accuracy on a Multisegment Tree

We illustrate the application of our approach on a six-segment tree where all horizontal and vertical segments are $20\mu\text{m}$ and $10\mu\text{m}$ long, respectively. The corresponding current densities are marked in Fig. 6(a). A uniform element length of $5\mu\text{m}$ is used for all segments: this results in 20 elements, implying that this is a 20^{th} order system. The transient values of the stress at an exemplar node, node 4, is shown in Fig. 6(b). In this case, the non-guaranteed-stable approximant from Step 1 provides all-stable left-half-plane poles for orders $p = 2, 3, \dots, 9$. The results for three orders are shown in the figure, and high accuracy is obtained for $p = 4$. Similar results are seen at all other nodes of the tree. Fig. 6(c) shows the results of the simulation at the whole tree, at two time instants, where the Step 1 and Step-2 plots overlap almost perfectly with the COMSOL generated plots at both time points. In all cases, Step 1 provides a stable solution, but for comparison, we also show the results of the provably stable Step 2 MOR method. The figure shows that the Step 1 results almost completely coincide with the numerical COMSOL result, but Step 2 results show some small inaccuracy. This loss of accuracy is the price paid for the stability guarantee, and we empirically observe this in several cases. This is why we use Step 1 as far as possible, going to Step 2 only when Step 1 fails.

B. Scalability Analysis

Table I shows the time cost of the proposed method for a sequence of T -junctions as shown in Fig. 7 [26]. For a structure with n junctions, each junction is a node and there are $2n + 1$ segments in the tree. Each horizontal and vertical segment is $20\mu\text{m}$ and $10\mu\text{m}$ long, respectively. A uniform element length of $5\mu\text{m}$ is chosen. The table shows t_{dis} , the runtime to build the system matrices resulting from the discretization; t_{mom} , the runtime for computing the moments using forward and reverse traversals for an order of $p = 4$; t_{MOR} , the runtime for model order reduction; t_{σ} , the time required to simulate the reduced-order model; and t_{Total} , the total runtime. The runtime scales along the expected near-linear trend for larger interconnect trees, as evident from the reported total runtime and its components in Table I. For all structures in Table I, Step 2 is never invoked. We report runtime speedups for the structures in [26] on a comparable machine: our approach is an order of magnitude faster.

C. Analysis on IBM Power Grid Benchmarks

We apply our approach to the IBM power grid benchmarks [27]. These benchmarks are simulated using SPICE to extract branch currents in every wire. Since these benchmarks do not specify the widths and thicknesses of segments in the grid, we back-calculate the product of the segment width and thickness (cross-sectional area).

We model the connectivity of each benchmark using a graph, where the nodes correspond to junctions, end-points,

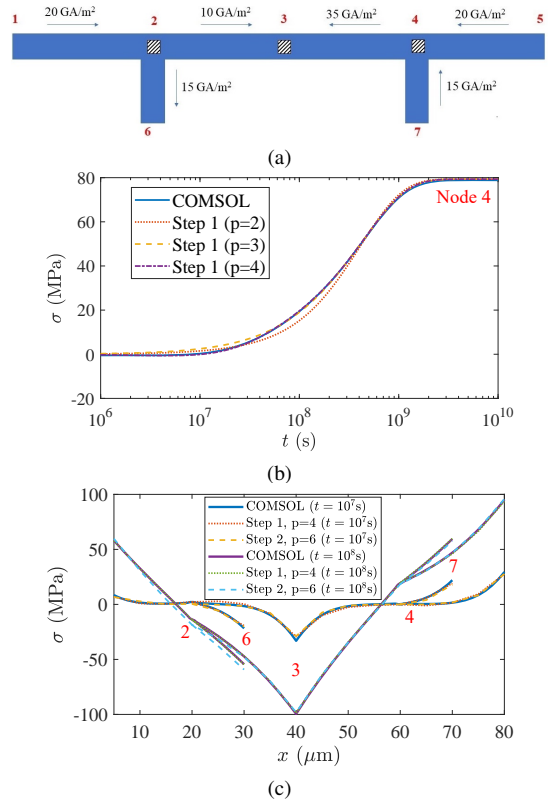


Fig. 6: (a) A six-segment interconnect tree. (b) Transient stress at node 4 tree for multiple orders of MOR using Step 1. (c) Spatial stress profile at two time instants for both Step 1 and Step 2 (x is the distance from node 1 [node 2 at $x = 20$, node 3 at $x = 40$, etc.]).

or vias, and the edges are the power stripes that connect adjacent nodes. Since each benchmark contains multiple voltage domains and nets (Vdd and Vss), we first traverse the power grid graph to identify connected components and extract tree structures. We discretize each edge of the tree into elements of size $\Delta x = 10\mu\text{m}$; for wires whose lengths are not multiples of $10\mu\text{m}$, we consider the remainder of the wire length to be



Fig. 7: An interconnect structure with n T -junctions.

TABLE I: Runtime of our proposed algorithm on an interconnect structure with n T -junctions (Figure 7).

n	Runtime (sec)					Speedup over [26]
	t_{dis}	t_{mom}	t_{MOR}	t_{σ}	t_{Total}	
100	0.006	0.007	0.021	0.009	0.043	13×
200	0.011	0.015	0.062	0.017	0.105	11×
500	0.029	0.035	0.117	0.038	0.219	13×
1000	0.053	0.064	0.221	0.019	0.357	17×
2000	0.088	0.442	0.311	0.033	0.874	14×
10000	0.498	1.158	1.493	0.161	3.31	20×
20000	1.005	2.007	4.196	0.311	7.52	(not reported in [26])
50000	2.635	4.800	18.350	0.767	26.56	11×

TABLE II: IBMPG benchmarks: EM mortality statistics and runtimes using our algorithm (#nodes after discretization).

	# trees	# wires	# nodes	# elements	# trees w/ Step 2 solution	# mortal wires after			CPU time (s)
						3y	5y	10y	
pg1	1.2K	30K	0.9M	0.9M	0	46	63	94	39
pg2	1.2K	126K	0.7M	0.7M	0	0	0	3	42
pg3	15K	835K	8.1M	8.1M	6	2	5	14	484
pg4	20K	932K	4.3M	4.3M	4	0	0	0	300
pg5	3K	108K	4.9M	4.9M	0	0	0	0	330
pg6	21K	165K	3.5M	3.4M	24	59	164	658	432

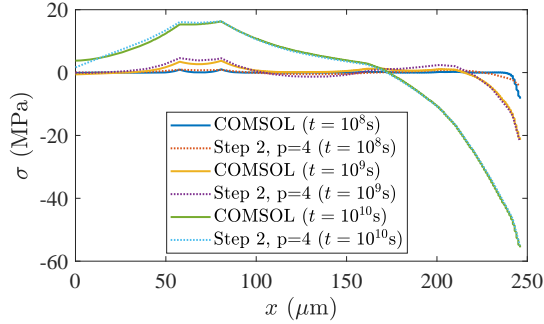


Fig. 8: Guaranteed stable (Step 2) stress profile of a 14-segment ibmpg6 wire, where the Step 1 solution is unstable.

an independent smaller element. Table II lists the number of trees⁵ in the benchmark, the number of wires, and the number of nodes and elements after discretization for all benchmarks.

Next, we apply our approach to each tree structure using $p = 4$ for the reduced-order models. We report the number of trees that have no Step 1 solution because of passivity issues (for which Step 2 was invoked), and we compute stress at the end points of every wire for three different lifetimes (3, 5, and 10 years). We list the number of mortal wires for different lifetimes and the total runtime to compute the transient stress using our proposed approach. As in Section V-B, the runtime is the sum of t_{dis} , t_{mom} , t_{MOR} , and t_{σ} . The method is fast, taking eight minutes to compute transient stress on the pg3 benchmark with $>8M$ nodes after discretization). For pg4 and pg5, we find no mortal segments for all three lifetimes which is consistent with [8]. In addition, we also observe a few rare tree structures (34 trees out of a total of 62K trees, or 0.05%), in which the Step 1 solution gives right-half-plane poles and is unstable, and where the guaranteed stable Step 2 solution is invoked. The small number of invocations of Step 2 has no discernible impact on the runtime.

Fig. 8 shows the Step 2 solution for a stripe in pg6 that has no stable Step 1 solution. The stress profile agrees with COMSOL, but slight differences are seen due to the accuracy-stability tradeoff.

VI. CONCLUSION

We use stress-electrical equivalence and apply model order reduction methods to solve for EM-induced stress in a multisegment line. We solve the problem using a Krylov

⁵Note that the number of trees is larger than the number of trees reported by [14], [26] as we report numbers for both Vdd and Vss nets.

subspace method that uses tree traversals to achieve a linear-time solution of the transient stress in tree-structured interconnects, which has never been previously demonstrated. The formulation is general enough to be extended to post-voiding models [17], [28]. This is a topic for future work.

REFERENCES

- [1] S. M. Alam, *et al.*, “Circuit-level reliability requirements for Cu metallization,” *IEEE T. Device Mater. Rel.*, vol. 5, pp. 522–531, 2005.
- [2] C. Auth, *et al.*, “A 10nm high performance and low-power CMOS technology featuring 3rd generation FinFET transistors, self-aligned quad patterning, contact over active gate and cobalt local interconnects,” *Proc. IEDM*, 2017.
- [3] I. A. Blech, “Electromigration in thin aluminum films on titanium nitride,” *J. Appl. Phys.*, vol. 47, no. 4, pp. 1203–1208, 1976.
- [4] J. R. Black, “Electromigration failure modes in aluminum metallization for semiconductor devices,” *Proc. IEEE*, vol. 57, pp. 1587–1594, 1969.
- [5] M. A. Korhonen, *et al.*, “Stress evolution due to electromigration in confined metal lines,” *J. Appl. Phys.*, vol. 73, pp. 3790–3799, 1993.
- [6] E. Demircan and M. Shroff, “Model based method for electro-migration stress determination in interconnects,” *Proc. IRPS*, 2014.
- [7] F. Najm and V. Sukharev, “Electromigration simulation and design considerations for integrated circuit power grids,” *Journal of Vacuum Science & Technology B*, vol. 38, pp. 063204:1–12, Nov/Dec 2020.
- [8] M. A. A. Shohel, *et al.*, “A new, computationally efficient ‘Blech criterion’ for immortality in general interconnects,” *Proc. DAC*, 2021.
- [9] H.-B. Chen, *et al.*, “Analytical modeling and characterization of electromigration effects for multibranch interconnect trees,” *IEEE T. Comput. Aid D.*, vol. 35, pp. 1811–1824, 2016.
- [10] H.-B. Chen, *et al.*, “Analytical modeling of electromigration failure for VLSI interconnect tree considering temperature and segment length effects,” *IEEE T. Device Mater. Rel.*, vol. 17, no. 4, pp. 653–666, 2017.
- [11] V. Mishra and S. S. Sapatnekar, “The impact of electromigration in copper interconnects on power grid integrity,” *Proc. DAC*, 2013.
- [12] V. Mishra and S. S. Sapatnekar, “Predicting electromigration mortality under temperature and product lifetime specifications,” *Proc. DAC*, 2016.
- [13] B. Li, *et al.*, “Statistical evaluation of electromigration reliability at chip level,” *IEEE T. Device Mater. Rel.*, vol. 11, pp. 86–91, Mar. 2011.
- [14] S. Chatterjee, *et al.*, “Power grid electromigration checking using physics-based models,” *IEEE T. Comput. Aid D.*, vol. 37, pp. 1317–1330, July 2018.
- [15] C. Cook, *et al.*, “Fast electromigration stress evolution analysis for interconnect trees using Krylov subspace method,” *IEEE T. VLSI Syst.*, vol. 26, pp. 969–980, 2018.
- [16] M. A. A. Shohel, *et al.*, “Analytical modeling of transient electromigration stress based on boundary reflections,” *Proc. ICCAD*, 2021.
- [17] F. N. Najm, “Equivalent circuits for electromigration,” *Microelectronics Reliability*, pp. 114200–1–114200–16, Aug. 2021.
- [18] J. Gambino, “Process technology for copper interconnects,” in *Handbook of Thin Film Deposition* (K. Seshan and D. Schepis, eds.), ch. 6, pp. 147–194, Amsterdam, The Netherlands: Elsevier, 3rd ed., 2018.
- [19] L. Zhang, *et al.*, “Grain size and cap layer effects on electromigration reliability of Cu interconnects: Experiments and simulation,” in *AIP Conf. Proc.*, vol. 1300, 3, 2010.
- [20] M. N. Özişik, *Heat Transfer: A Basic Approach*. New York, NY: McGraw-Hill, 1985.
- [21] M. Celik, *et al.*, *IC Interconnect Analysis*. Boston, MA: Kluwer, 2002.
- [22] S. Sapatnekar, *Timing*. New York, NY: Springer, 2004.
- [23] H. B. Bakoglu, *Circuits, Interconnections and Packaging for VLSI*. Reading, MA: Addison-Wesley, 1990.
- [24] A. Odabasioglu, *et al.*, “PRIMA: Passive reduced-order interconnect macromodeling algorithm,” *IEEE T. Comput. Aid D.*, vol. 17, pp. 645–654, 1998.
- [25] L. Pillage and R. Rohrer, “Asymptotic waveform evaluation for timing analysis,” *IEEE T. Comput. Aid D.*, vol. 9, pp. 352–366, 1990.
- [26] X. Wang, *et al.*, “Fast physics-based electromigration analysis for full-chip networks by efficient eigenfunction-based solution,” *IEEE T. Comput. Aid D.*, vol. 40, pp. 507–520, 2021.
- [27] “IBM power grid benchmarks.” <https://web.ece.ucsb.edu/~lip/PGBenchmarks/ibmpgbench.html>, Accessed May 21, 2023.
- [28] V. Sukharev, *et al.*, “Postvoiding stress evolution in confined metal lines,” *IEEE T. Device Mater. Rel.*, vol. 16, pp. 50–60, 2016.